Silicon surface functionalization based on cavitation processing

R.K. Savkina[a,*], A.B. Smirnov[a], A.I. Gudymenko[a], V.A. Morozhenko[a], A.S. Nikolenko[a], M.I. Smoliy[a], T.G. Kryshtab[b]

[a] *V. Lashkaryov Institute of Semiconductor Physics, National Academy of Sciences of Ukraine, 41 Nauky av, Kyiv 03028, Ukraine*
[b] *Instituto Politécnico Nacional - ESFM, Department of Physics, Av. IPN, Ed. 9 U.P.A.L.M., 07738, Mexico City, Mexico*

ARTICLE INFO

ABSTRACT

Functionalization of semiconductor substrates, specifically silicon, has focused attention toward such technological applications as photovoltaic and biosensing. Several common chemical approaches have been employed for this purpose. In this paper, we focus on the alternative approach dealing with ultrasound-assisted modification of silicon. The aim was to identify the chemical functional groups and to evaluate the biocompatibility of the ultrasonically processed semiconductor. The properties of the Boron-doped *p*-type (100) silicon wafers subjected to cavitation impacts have been studied. It was shown that high-intensity ($15\,W/cm^2$) and high-frequency ($1 \div 6\,MHz$) sonication of silicon wafers in the liquid nitrogen in focused mode of acoustic action induces changes of the optical, chemical, and structural properties of semiconductor surface. The cavitation processing of the Si samples besides a structuring of semiconductor surface and possible phase transformation of bulk material, results in the formation of functional oxide layers consisted of such materials as SiO_2, $CaSiO_3$ and Ca_2SiO_4. The formation of a new phase on the silicon surface is confirmed by the results of X-ray diffraction and μ-Raman spectroscopy investigations. The obtained composite structure has demonstrated photoluminescence in the spectral range of 500–800 nm. Biocompatibility of the ultrasonically processed wafers was confirmed by the hydroxyapatite formation on the Si surface after storage in simulated body fluid solution.

1. Introduction

Semiconductors as substrates for functional materials have been developed into an active field of research at the interface between physics, chemistry and biology. Their surface modification has a wide range of applications in the fields of micro- and nanotechnology, optoelectronics, biosciences and biotechnologies, etc. Among all semiconductors, silicon remains as a key element in the area of the high-technology electronic devices fabrication [1]. An effective way to expand its practice is developing of the new composite and hybrid Si-based systems, joining diverse materials, which allows the integration of several key functions in a single structure and more complex properties for the new devices. For example, a device that combines a conventional silicon cell with a perovskite (such as $CH_3NH_3PbI_3$ [2], $[HC(NH_2)_2]_{0.83}Cs_{0.17}Pb(I_{0.6}Br_{0.4})_3$, [3]) to increase the efficiency by converting more sun's energy into electricity has already been created. At that, the efficiency of such devices can be increased up to 25% or even to 30% [4]. Silicon-based hybrid organic-inorganic structures have also received most of the attention in the field of bio-interfacing [5]. Thereby, state of the semiconductor surface, particularly silicon surface, performs a significant role both for photovoltaic and biosensing applications.

A common need for all electronic devices requires the density of electronic defect states at the Si surface $< 10^{12}\,cm^{-2}$, and the Si/organic interface should be stable in humid environments [6]. Silicon surface properties adjustment is usually carried out by chemical routes. Surface functionalization of silicon has initially focused on functionalization of OH-terminated silicon oxide surfaces, using silanization, which strongly depends on the density of initial surface OH groups, the number of water molecules present, and the temperature [6]. Functionalization of oxide-free silicon surfaces makes it possible to construct more efficient structures, as this approach significantly reduce the density of defect states and traps on semiconductor interface. A simple and rapid surface functionalization for H-terminated Si(111) surfaces using alkyl silanols is presented in [7].

Alternative methods of the Si surface modification are based on thermal activation or visible light irradiation. One of the alternatives is the sonochemical approach. Extreme conditions of the ultrasonic cavitation such as local temperature and pressure are widely used in chemistry, as for example to synthesize nano-materials, to enhance the electrochemical reactions and to modify the surface properties of electrodes [8,9]. The ultrasonic irradiation is a powerful tool for

---

promotion of the chemical reactivity in the liquids at the solid surfaces. In our previous works [10,11], we focused on an attempt to drive the chemical and structural transformations on silicon surface by the ultrasonic (US) cavitation effect. It was found that the cavitation processing of the silicon samples has resulted in the essential change of the surface morphology as well as optical and structural properties of semiconductor. After 15 ÷ 30 min of sonication, inside the structured region nano- and subnanoscale objects as well as dendrite-like objects were revealed. The further increase of processing time results in the appearance of the features with crystal symmetry. Based on μ-Raman and SPV spectroscopy results, we have demonstrated an improvement of the photoelectric properties and a new chemical phase formation on silicon surface exposed to the MHz sonication in the liquid nitrogen medium. The purpose of the present paper is to identify the formed chemical functional groups and to evaluate biocompatibility of the ultrasonically processed semiconductor.

2. Experimental

2.1. Samples

Silicon samples were cut into 5 mm × 5 mm square from the boron-doped (100)-oriented *p*-type silicon wafers of diameter about 76.2-mm grown by the liquid-encapsulated Czochralski method. They were cleaned for 10 min in ethanol and then in ddH$_2$O (water for analytical laboratory use, ISO 3696:1987). The initial surface was found to be flat, devoid of defects, with a measured roughness lower than 1 nm. The roughness was determined by atomic force microscopy (AFM) at a few randomly chosen areas of 40 × 40 μm^2. XRD patterns for the initial samples denote the existence of a small amount of amorphous phase on the Si substrate surface investigated (broad bump intensity distribution in the range of $2\theta = 20$–$30°$, see part 3.3). We believe that this layer is removed during the sonication since the modified region is integrally below the original surface.

2.2. Cavitation processing

All samples were treated by the cavitation impact in cryogenic liquid such as nitrogen (LN$_2$). For the cavitation activation, we used a high frequency system (MHz) with focused energy resonator [12]. Utilization of the focusing in our experiment has allowed increasing power of the high-frequency acoustic system as well as concentrating the exposure on the exact position of the solid surface so as not to affect surrounding regions. It should be noted that the effective cavitation nucleation is due to the fact that the operating temperature in the US reactor is close to the boiling point of nitrogen. Moreover, the presence of the dust particles in the technical nitrogen as well as microscopic vapour bubbles caused by the heat release due to non-ideal thermal insulation in the experimental vessel also facilitate the process of the cavitation excitation.

A pumped stainless steel tank with internal copper cell filled with LN$_2$ was used for the reactor vessel (see Fig. 1). A ceramic piezoelectric transducer (PZT-19) with a diameter of 12 mm and a resonant frequency of 3 MHz (or 6 MHz) acoustically drove the cell. A cylindrical copper concentrator (lens) was used for US intensity enhancement. Intensity gain of the acoustic system (PZT + copper lens) was estimated as [13]:

$$k_I = \frac{4Ff_{US}}{c_1} \sin\gamma,$$

(1)

where f_{US} is an ultrasonic frequency, γ is an opening angle of a wave front, c_1 is an acoustic impedance of the LN$_2$, and F is a focal distance:

$$F = R_{cu}\left(1 + \frac{n^2}{1 - n^2}\cos\beta\left(1 + \sqrt{1 + \frac{1 - n^2}{n^2}\cos\beta}\right)\right)$$
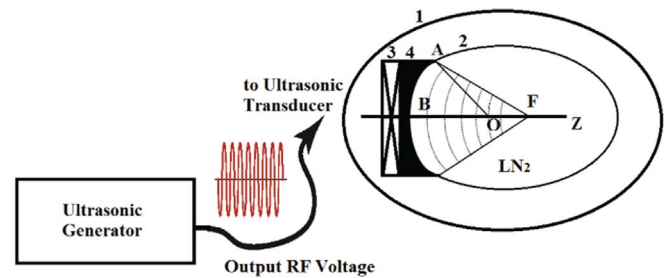
(2)

Fig. 1. A schematic image of the ultrasonic cell (top view): stainless steel tank (1) with internal copper cell (2) equipped with an acoustic system – a piezoelectric transducer (3) and copper lens (4); AO = R_{cu}, AF = F, ∠AOB = β, ∠AFB = γ. The output voltage of US generator did not exceed 5 V, and the initial value of the acoustic intensity W_{US} did not exceed 1 W/cm^2. Schema is adapted with permission from ref. [14]. © Springer International Publishing 2016.

$$n = \frac{c_1}{c_2}$$

(3)

where R_{cu} is a curvature radius, c_2 is an acoustic impedance of copper, $\beta = $ ∠AOB (see Fig. 1). Intensity gain of the acoustic system estimated according to Eq. 1 was about 58. The acoustic matching of the PZT to copper lens is sufficient for satisfying the condition of transparent boundary ($\sim 98\%$). But the value of the acoustic impedance ratio estimated according to Eq. 3 is about 0.02 and, as a consequence, the ratio of the emitted acoustic power to the dissipated power is $\sim 55\%$. The maximal value of pressure was about ~ 8 bar in the focus of the acoustic system.

2.3. Fabrication of Si/SiO$_2$/CaSiO$_3$ composite

Semiconductor target was placed inside the acoustically driven copper cell in the focus region (see Fig. 1). The powder of gluconic acid calcium salt C$_{12}$H$_{22}$CaO$_{14}$was added to the reactor vessel. Its heat decomposition during the cavitation processing leads to the formation of calcium oxide CaO, carbon C, carbon dioxide CO$_2$ and water H$_2$O. After sonication some samples were annealed in the nitrogen vapour at 1100 °C for 2 h. Another group of samples were annealed in the atmospheric ambient at 980 °C for 1 h. The samples were cooled to room temperature in the furnace.

2.4. Evaluation of Si surface biocompatibility

The biocompatibility of the ultrasonically processed Si surfaces was evaluated by examining the bone-like apatite formation on the samples in simulated body fluid (SBF), which had similarity of concentrations to those in human blood plasma. The process of dissolving reagent grade chemicals: KCl, NaCl, NaHCO$_3$, K$_2$HPO$_4$·3H$_2$O, MgCl$_2$·6H$_2$O, CaCl$_2$ and NaSO$_4$ was carried out according the method described in [15]. The buffer solution was prepared using tris-(hydroxymethyl)aminomethane. The pH of SBF was maintained at 7.4 using 1 M solution of HCl. Each Si sample was soaked in the SBF during 30 days at 36.7 °C. Every 7 days, the SBF solution was refreshed. Before further characterization, the samples were removed from the SBF solution, rinsed with be-distilled water and dried at room temperature.

2.5. Characterization of the processed samples

All processed surfaces were examined using Digital Instruments NanoScope IIIa. The IR spectra of the samples after cavitation processing were obtained with an Infralum FT-801 Fourier IR spectrometer in the range of 500–5000 cm^{-1} with resolution of 2 cm^{-1}. The optical parameters (extinction coefficient k and refractive index n) and thickness d of the surface layers on silicon substrate after cavitation processing were controlled by ellipsometry using an LEF 3 M-1 laser

photoelectron self-compensating null-ellipsometer (λ = 632.8 nm). The ellipsometric parameters Δ and ψ were determined from the results of multi-angle measurements in a range of incidence angle ϕ = 50°–75°.

Grazing incidence X-ray diffraction was applied to obtain two-dimensional crystallographic information parallel to the sample surface. XRD patterns were obtained by using ARL X'tra (Thermo scientific) X-ray diffractometer with Cu K_α radiation. Also high resolution X-ray diffraction (HRXRD) was used to investigate the deviation from ideal structure of Si along the surface normal. X-ray rocking curves and symmetric ω-2θ scan for samples investigated before and after the sonication were obtained using a Panalytical X'Pert-Pro triple-axis X-ray diffractometer. The Cu $K_{\alpha 1}$ line with a wavelength of 0.15418 nm was selected using a four-bounce (440) Ge monochromator. The experimental schemes allowed two cross-sections of reciprocal lattice sites to be obtained: normally (ω-scanning) and in parallel (ω/2θ-scanning) to the diffraction vector.

Micro-Raman spectra were measured in backscattering geometry at room temperature using triple Raman spectrometer T-64000 Horiba Jobin-Yvon, equipped with cooled charge-coupled device detector. The line 488 nm of Ar−Kr ion laser was used for excitation. Exciting radiation with power of 1–2 mW was focused on the sample surface to the spot of 1 μm in diameter.

3. Results and discussion

3.1. Surface evolution

The AFM images of the samples investigated are shown in Fig. 2 that demonstrate the morphological evolution of the sonicated Si surface with the treatment duration. In panel A of the Fig. 2 the morphology of Si surface after 10 min treatment in LN_2 is shown. Disordered nanostructured relief with the characteristic height $h \sim 10$ nm is observed (see the corresponding histogram). Images were processed with WSxM software [16]. The relative increase of the roughness of the surface quantified using root-mean-square (RMS) average of height deviations

parameters as well as the increase of the average absolute deviations parameter (R_a) is observed with the duration of the acoustic cavitation. For example RMS roughness is ~ 5 nm and the parameter R_a is ~ 3.8 nm after 10 min treatment, RMS roughness increases up to ~ 33 nm and the parameter R_a increases up to ~ 27 nm after 20 min treatment, after 35 min treatment the value of RMS roughness is ~ 98 nm and the value of parameter R_a is ~ 79 nm. The increase in the processing time of 20 min gives rise to emergence of nano-islands with the characteristic height $h \sim 80$ nm and with a base diameter of 200 to 300 nm (see Fig. 2b). The further increase in the processing time results in the rise of a number, as well as height and lateral sizes of these objects (see Fig. 2c and the corresponding histogram).

It should be noted that silicon is known as a very brittle material, which must be deformed by cracking under the influence of the collapsing bubbles [17]. Silicon has a brittle-to-ductile transition at around ~ 500 °C. However, we have not observed any cracking after Si surface treatment. In our opinion, this may be due to the size effect of brittle-to-ductile transition during nanoscopic compression of silicon described in Ref. 18. The critical size is between 300 and 400 nm. Indeed, the study of the bubbles dynamics in the frame of the Rayleigh-Plesset equation has shown that the mean radius R of the cavitating bubble at a MHz frequency cavitation is in the subnanometer range in contrast to tens of μm in radius R at kilohertz (kHz) frequency cavitation. For example, $R = 300$–600 nm for argon and xenon at $f_{US} = 1$ MHz [19]. So, the minimum radius of the collapsing bubble, caused by the Van der Waals hard-core volume, is reduced to the value $\sim R/9$, i.e. is smaller than the critical size of the mentioned effect.

3.2. Optical properties investigation

It was found that ultrasonically structured regions of silicon surface demonstrate the photoluminescence (PL) response in the range of 500 to 900 nm, with an intense peak around 565 nm (2.2 eV) and 750 nm (1.65 eV) (see Fig. 3). It should be noted that before annealing, we observed the lower energy PL band in the region of 1.7 eV. PL bands of the sonicated samples after annealing at 980 °C in the atmospheric
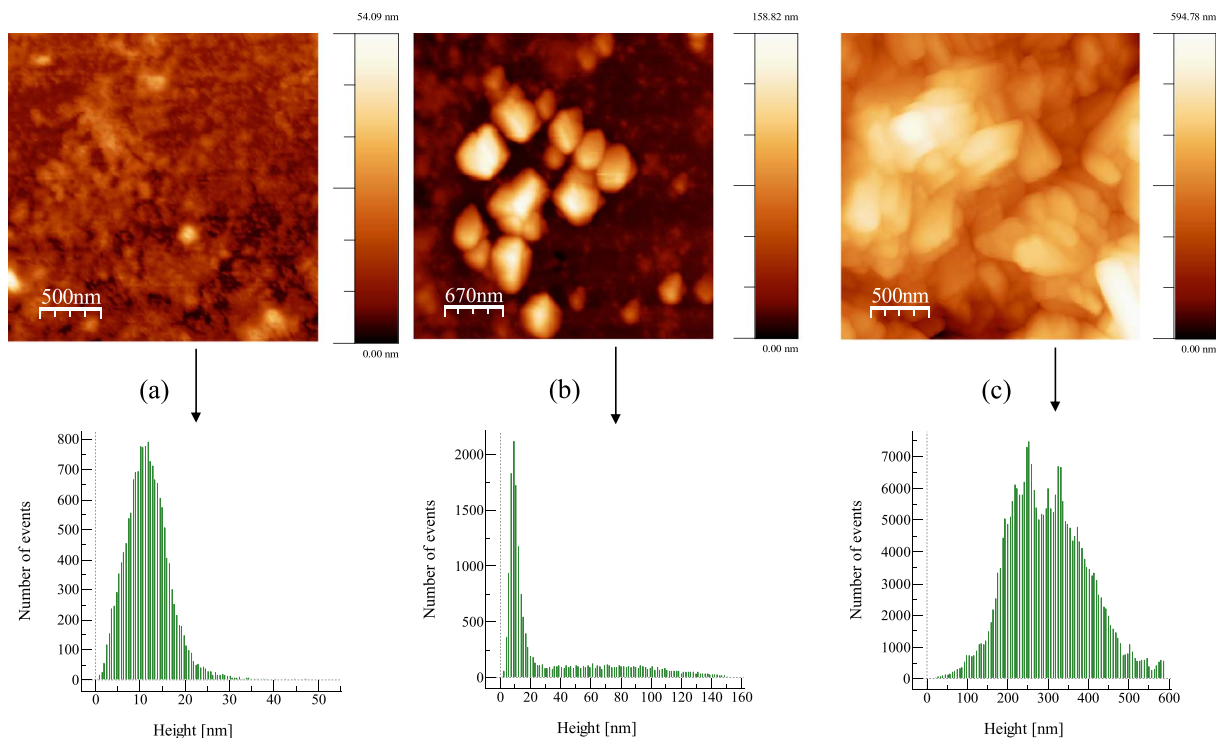

Fig. 2. Typical AFM images of the surface evolution during the (1–6) MHz sonication (15 W/cm²) with corresponding histograms for Si samples: (a) - 10 min treatment in LN_2, (b) – 20 min treatment in LN_2, (c) - 35 min treatment in LN_2.
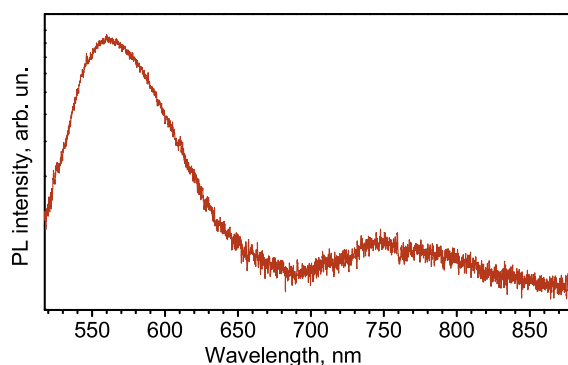
Fig. 3. Photoluminescence spectrum of Si surface sonicated in the LN_2 (488 nm of Ar–Kr laser).

ambient are shown in Fig. 3. However, silicon samples, sonicated and annealing at 1100 °C in an inert atmosphere, have demonstrated PL band around 2.2 eV only.

PL bands in the energy range of 2.1–2.3 eV and around 1.7 eV are generally observed in *Si*-rich SiO_x (x < 2) matrixes prepared by various techniques such as PECVD [20], implantation of silicon into silica [21] or thermal evaporation of silicon monoxide in vacuum [22]. At that, the properties of the PL bands appear to be very complex and strongly depend on the oxygen content in the SiO_x. The most researchers agree that PL band at the higher energy (2.1–2.3 eV) is the result of the defect luminescence, possibly from non-bridging oxygen centers or related oxygen vacancies. The lower energy PL band (around 1.7 eV) is associated with radiative recombination of confined excitons.

PL bands observed in our experiment could also be related to the radiative processes in silicon oxide. The investigation of the chemical composition of the ultrasonically structured silicon surface (studied by SEM equipped with EDAX) indicates its oxidation with weight percent of the oxygen in some areas up to 12% [10,11]. In the works mentioned, we have also found that cavitation treatment with post-annealing of Si samples leads to the formation of a complex optical system with several transition layers. And at least one of them is characterized by optical parameters close to silicon oxide. The characteristics of these layers depend on the annealing conditions that can be the subject of a separate investigation. Here we note only some features. Namely, for samples sonicated and annealed in the atmospheric ambient at 980 °C, subsurface layer adjoining to a substrate may be associated with the formation of *Si*-rich SiN_x compound according to Refractive index database (refractive index $n \sim 3.12$) [23]. Its thickness reaches 500–900 nm. Top layer with the thicknesses of 100 to 150 nm has refractive index ($n \sim 1.46$) and extinction coefficient ($k \rightarrow 0$) at $\lambda = 632.8$ nm close to SiO_2 compound [10]. At the same time, samples sonicated and annealed in the nitrogen vapour at 1100 °C demonstrate the formation of the layer with the thicknesses of ~ 700 nm and optical parameters closed to SiO_2 compound [11]. And, the accurate numerical interpretation of the ellipsometer results became possible only after introducing an additional top layer with the thicknesses ~ 15 nm and the refractive index ~ 1 during optical modeling.

3.3. XRD analysis

A phase composition of the surface layers of the sonicated and annealed Si samples was studied by using X-ray diffraction in the grazing geometry (the angle of incidence for the incoming X-ray was 5˚). Fig. 4a shows the XRD patterns of the typical initial and processed Si samples. Against the broad bump intensity distribution that corresponds to the presence of an amorphous layer at the sample surface, XRD patterns reveal series of diffraction peaks, which correspond to reflections from SiO_2, $CaSiO_3$ and Ca_2SiO_4 compounds. Polymorphs of SiO_2 as quartz, cristobalite and stishovite were found after sonication and annealing

(see also Table 1). Calcium silicate $CaSiO_3$ was formed with both orthorhombic and monoclinic crystal structures as well as with stable at ambient pressure triclinic crystal structure. Calcium orthosilicate Ca_2SiO_4 was formed with orthorhombic crystal structure after cavitation processing and subsequent annealing in the atmospheric ambient at 980 °C for 1 h only. Table 1 presents the information of the synthesized compounds on silicon surface with corresponding crystallographic planes, crystal system and space group.

Figs. 4b and c show HRXRD results for typical sonicated and annealed at 1100 °C sample. It is seen the increase of background in the direction parallel to the diffraction vector, which is demonstrated by the increase in the FWHM parameter of the ω–2θ scans from 20.6 arcsec for initial samples to 21.9 arcsec - for US processed and to 27.3 arcsec - for annealed at 1100 °C samples (see Fig. 4b). This indicates the presence of deformation in the direction normal to the surface. Similar processing also increases the diffuse scattering region in the direction perpendicular to the diffraction vector, which is demonstrated by the increase in the FWHM parameter of the ω scans (see Fig. 4c). Formally, in can mean the formation of lateral strains.

The lattice parameters of the processed silicon are calculated to be $a = 5.43089$ Å for samples annealed at 980 °C and $a = 5.43101$ Å - for samples annealed at 1100 °C. These parameters are lower than the results for initial sample ($a_o = 5.43129$ Å) and points to a compressive strain in the semiconductor lattice in the direction normal to the surface after the cavitation processing and the annealing. It should be noted that the presence of coupled layers on the silicon surface with different structure parameters could be the reason of the lattice strain and the diffuse scattering change.

3.4. μ-Raman and FTIR investigations

A close inspection of the μ-Raman spectra of Si samples investigated exhibit a cubic diamond structure (space group Fd-3 m) characterized by a one first-order Raman active phonon located at the center Γ point of the Brillouin zone corresponding to a phonon wave vector ~ 520 cm^{-1} with full width at half maximum $\Delta_{FWHM} \sim 3.8$ cm^{-1} (see Fig. 5). The first-order scattering from transfer TA(L) acoustical phonons and from optical phonon LO(L) as well as the second-ordered scattering from transfer 2TA acoustical phonons [24] are observed. The values of the corresponding frequencies are presented in Table 2. The peak at 620 cm^{-1} probably corresponds to the combination TO(X) + TA(X) modes, and the weaker peak at 670 cm^{-1} corresponds to TO (Σ) + TA (Σ) [25].

After sonication and annealing at 980 °C, it was found a broadened LO-TO(Γ) Si band, with a measured full width at half-maximum up to $\Delta_{FWHM} \sim 4.54$ cm^{-1} (see Fig. 5, spectrum b). Its line shape becomes asymmetric with a little tail on the low-energy side which indicates a partial amorphous-like structure. Wide and low-intensity band at 150 cm^{-1} indicates the appearance of an amorphous phase also (depicted by asterisk in spectrum b, Fig.5). At the same time, LO-TO peak broadening as well as appearance of an amorphous phase are not observed on the μ-Raman spectrum after an annealing at 1100 °C (see Fig. 5, spectrum c).

For silicon samples after sonication and annealing, it was detected an appearance of the local vibrational modes characterized wollastonite form of $CaSiO_3$. Spectrum of wollastonite obtained from the RRUFF database [26] is presented in Fig. 5 as reference. Ca–O local vibrational mode at about 336 cm^{-1} and 412 cm^{-1} and Raman features at 642 cm^{-1} and 971 cm^{-1} corresponded the stretching vibration of the monomer SiO_4 and the stretching vibration of the chain SiO_4 tetrahedron respectively are observed [27].

Fig. 6 presents the Fourier-transform infrared (FTIR) spectra of the silicon samples after sonication and annealing. According to [28], depicted by numeral vibration modes are associated with β-$CaSiO_3$. Besides, spectrum of wollastonite obtained from the NIST database [29] is presented in Fig. 6 for comparison with experimental. It is obvious that
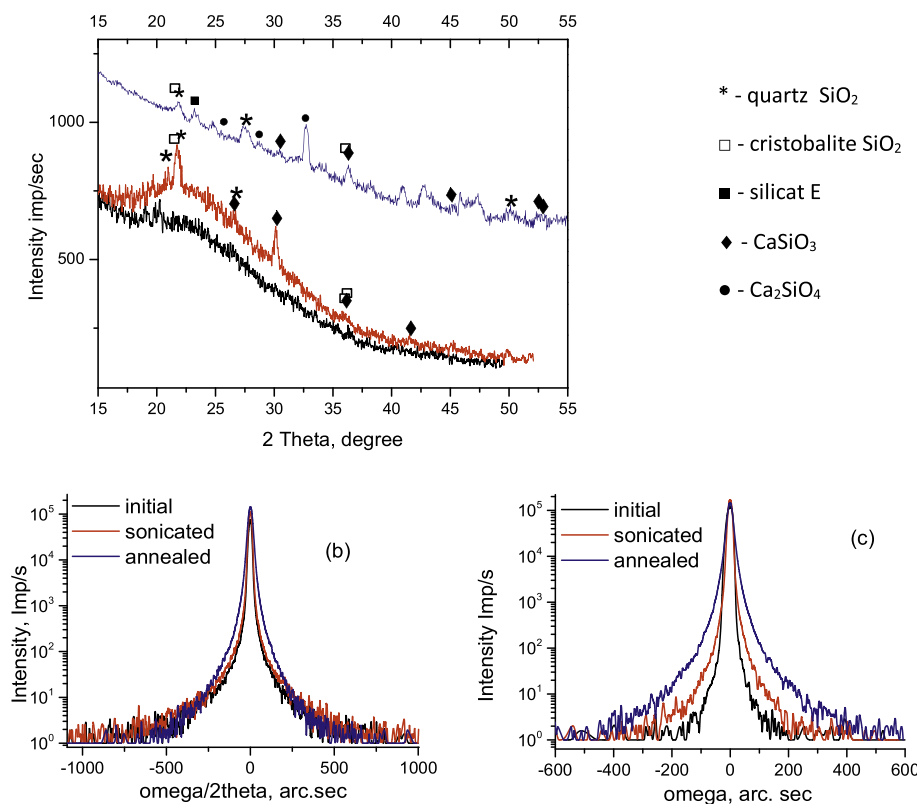
Fig. 4. (a) X-ray diffraction patterns of typical Si samples at initial state and after processing: 1 (black line) - the untreated silicon sample; 2 (red line) -silicon sample after sonication and annealing at 1100 °C; 3 (blue line) - silicon sample after sonication and annealing at 980 °C.
(b) (004) HRXRD omega/2theta diffraction profiles for typical sonicated and annealed at 1100 °C sample.
(c) (004) HRXRD omega diffraction profiles for typical sonicated and annealed at 1100 °C sample. (For interpretation of the references to colour in this figure legend, the reader is referred to the web version of this article.)

Table 1
Annealing conditions of Si samples after cavitation processing (1), compounds formed on Si surface after the cavitation processing and the annealing (2) and their crystal system, space group, diffraction peaks positions with corresponding crystallographic planes (3).

(1) Conditions	(2) Materials	(3) Crystal systems and space groups		
$T = 980$ °C $t = 1$ h	SiO_2	Quartz HP hexagonal, $P3_121$ $2\theta = 27.803°$ (101), $2\theta = 21.9287°$ (100) hexagonal, $P3_221$ $2\theta = 27.507°$ (011), $2\theta = 21.636°$ (100)	Cristobalite low tetragonal, $P4_12_12$, $2\theta = 21.8646°$ (101)	
	$CaSiO_3$	Orthorhombic, *Imma* $2\theta = 36.2918°$ (121) (200), $2\theta = 52.0889°$ (202), $2\theta = 52.4387°$ (040), $2\theta = 36.0678°$ (002)		
	Ca_2SiO_4	Orthorhombic, *Pmnb* $2\theta = 32.6546°$ (211)		
$T = 1100$ °C $t = 2$ h	SiO_2	Quartz low HP hexagonal, $P3_121$ $2\theta = 26.7488°$ (011), $2\theta = 20.9546°$ (100)	Stishovite tetragonal, P4$_2$/mnm $2\theta = 30.1017°$ (110)	Cristobalite low tetragonal, $P4_12_12$ $2\theta = 21.8052°$ (101), $2\theta = 35.903°$ (200), $2\theta = 36.0209°$ (112)
	$CaSiO_3$	Monoclinic, $P2_1/a$ $2\theta = 29.9911°$ (320), $2\theta = 25.3025°$ (002), $2\theta = 28.87°$ (202)		

$CaSiO_3$ crystallizes on the Si surface as a result of the high-temperature annealing.

Thus, high-intensity (15 W/cm^2) and high-frequency (1 ÷ 6 MHz) sonication of silicon samples in the liquid nitrogen in a focused mode of acoustic action induces changes of the optical, chemical, and structural properties of semiconductor surface. Formation of $Si/SiO_2/CaSiO_3$ composite structure occurs. This is confirmed by the results of X-ray, μ-Raman and FTIR spectroscopy investigations. It was found, that proposed method of ultrasonic treatment in a focused mode of acoustic action does not lead to the destruction of the Si surface.

3.5. Evaluation of biocompatibility

Biocompatibility of the ultrasonically processed Si substrates was estimated by the hydroxyapatite (HA) formation in SBF solution. Such

material as hydroxyapatite $Ca_{10}(PO_4)_6(OH)_2$ is widely used for hard tissue regeneration due to their close chemical similarity to biological apatite present in human hard tissues. Apatite layer plays an essential role in the formation of tight bone bonding between the bioactive materials and the neighboring tissues, and has not been observed for nonbioactive materials [30].

The biocompatibility of the obtained composite structure was evaluated by examining bone-like apatite formation ability via SBF soaking method. Two double-side polished samples Si1 and Si2 were double faced ultrasonically processed in cryogenic cell. Then, sample Si2 was annealed and both samples were stored in SBF solution at 36.7 °C. Fourier-transform infrared spectroscopy was performed on the silicon substrates before and after sonication and after storage in SBF.

Transmission IR spectra of initial and processed samples are shown in Figs. 7a–c. Silicon sample investigated in the initial state (see Fig. 7a,
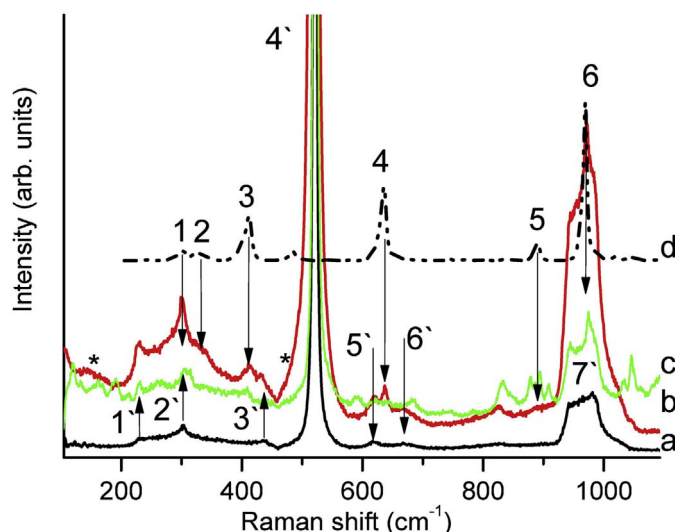
Fig. 5. *μ*-Raman spectra measured around localized defects after MHz sonication (15 W/cm^2, 35 min) and annealing:

a (Black solid line) - spectrum of the untreated silicon sample;

b (Red solid line) - spectrum of silicon sample after sonication and annealing at 980 °C;

c (Green solid line) - spectrum of silicon sample after sonication and annealing at 1100 °C;

d (Black dashed line) – spectrum of wollastonite obtained from the RRUFF database [26]

Numerals indicate the local vibration modes of silicon (1`–7`) and wollastonite (1–6). The values of the corresponding frequencies are given in Table 2. (For interpretation of the references to colour in this figure legend, the reader is referred to the web version of this article.)

Table 2
Local vibrational modes depicted in Fig. 5.

Silicon phonon frequencies			Wollastonite phonon frequencies		
1`	TA(L) [24]	230 cm^{-1}	1	–	303 cm^{-1}
2`	2TA(X) [24]	300 cm^{-1}	2	Ca−O [27]	335 cm^{-1}
3`	LO(L) [24]	430 cm^{-1}	3	Ca−O [27]	412 cm^{-1}
4`	Si(LO-TO)	520 cm^{-1}	4	Stretching vibration of the monomer SiO$_4$ [27]	642 cm^{-1}
5`	TO(X) + TA(X) [25]	620 cm^{-1}	5	–	890 cm^{-1}
6`	TO(Σ) + TA(Σ) [25]	670 cm^{-1}	6	Stretching vibration of the chain SiO$_4$ tetrahedron [27]	971 cm^{-1}
7`	2TO [24]	940–980 cm^{-1}			

curve 1) exhibits strong IR absorption band at 611 cm^{-1} assigned to a multiphonon absorption in the Si host as well as absorption associated with stretching (1107 cm^{-1}) and bending (817 cm^{-1}) vibration modes of the *Si*−O−Si bonds. The position of the stretching vibration mode changes with thermal annealing from 1107 cm^{-1} to 1080 cm^{-1}. Vibration mode at 885 cm^{-1} can be associated with sub-oxidized silicon species (oxygen interstitials) and is due to the structural combination of Si$_2$O$_3$. This peak position is almost constant with different treatments.

Transmission IR spectra of processed samples normalized on initial spectral distribution of transmission for spectral region from 400 to 1400 cm^{-1} are shown in Fig. 7b. Such suitable approach has permitted to eliminate the contribution from the substrate in the initial state. Fig. 7c shows transmission IR spectra of processed samples for spectral region from 2000 to 4500 cm^{-1}.

From the FTIR spectra depicted in Fig. 7b, any features are absent after sonication in the spectral region from 400 to 1400 cm^{-1}. The observed band around 2840 to 2960 cm^{-1} (see Fig. 7c) are attributed to the C−H stretching modes (2846 cm^{-1} ν_{as}CH$_2$, 2912 cm^{-1} ν_sCH$_2$, 2955 cm^{-1} νCH$_3$) [31]. Thermal annealing of the sonicated Si substrates results in the appearance of the weak absorption band between 790 and 830 cm^{-1} (Fig. 7b) and between 3250 and 3500 cm^{-1} (see Fig. 7c) which could be assigned to the N−H stretching modes [32].
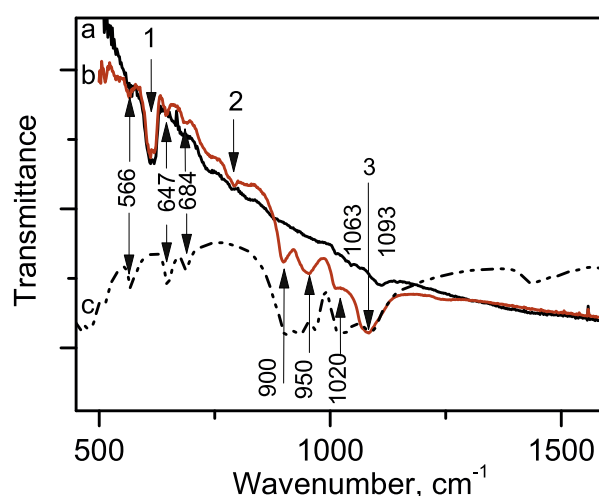

Fig. 6. FTIR spectra point out to sonochemical synthesis of calcium silicate on Si substrate:

a (black solid line) - spectrum of silicon sample after sonication;

b (red solid line) - spectrum of silicon sample after sonication and annealing at 1100 °C;

c (black dashed line) - spectrum of wollastonite obtained from the NIST database [29]. Numerically depicted vibration modes are associated with β-CaSiO$_3$ [28];

1 - Absorption band depicted around 614 cm^{-1} is associated with multiphonon absorption in Si host;

2 - N−H wagging [32]; 3 - absorption band around 1080 cm^{-1} could be connected with TO SiO$_2$ optical phonon mode [33]. (For interpretation of the references to colour in this figure legend, the reader is referred to the web version of this article.)

Strong absorption band around 1080 cm^{-1} with a shoulder at 1200 cm^{-1} could be connected with TO and LO SiO$_2$ optical phonon modes [33] and points out the crystallization of oxidized silicon surface as a consequence of thermal annealing.

Transmission IR spectra of silicon samples monthly stored in SBF solution demonstrate an appearance of the two optical bands associated with HA formation on the ultrasonically processed Si surface (depicted by Δ in Fig. 7b). Band around 550 cm^{-1} is assigned to HPO$_4^{2-}$ and PO$_4^{3-}$ groups and characteristic peaks at 960 cm^{-1} and 1030 cm^{-1} corresponds to the band of PO$_4^{3-}$ asymmetric stretching modes in HA [34,35].

It is necessary to note that Si samples both sonicated and sonicated with following annealing after storing in SBF solution during 30 days have demonstrated two strong optical bands corresponded to C−H and N−H vibrating modes (see Fig. 7c). Moreover, it was found that obtained functionalized layer exhibits antireflection properties in the MWIR and NWIR spectral ranges (see Fig. 7c). At last, on a control sample of silicon that was not subjected to cavitation processing, there was no formation of hydroxyapatite.

4. Conclusions

The method of the cavitation processing of semiconductor surface in a focused mode of acoustic action has been resulted in a change of the optical, chemical, and structural properties of semiconductor surface. The surface of bulk silicon is effectively functionalized with such materials as SiO$_2$, CaSiO$_3$ and Ca$_2$SiO$_4$. The obtained composite structure has demonstrated photoluminescence in the visible and NIR spectral range (500–800 nm). The formation of a new phase on the silicon surface is confirmed by the results of X-ray diffraction, μ-Raman and FTIR spectroscopy. It was found that proposed method of ultrasonic treatment does not lead to the destruction of the Si surface.

In vitro simulated body fluid soaking result showed that the fabricated Si/SiO$_2$/CaSiO$_3$ composite could induce formation of bone-like apatite layers. The FTIR investigation displayed the surface chemistry and confirmed that silicon substrate was effectively modified with bioactive material as well as C−H and N−H groups.
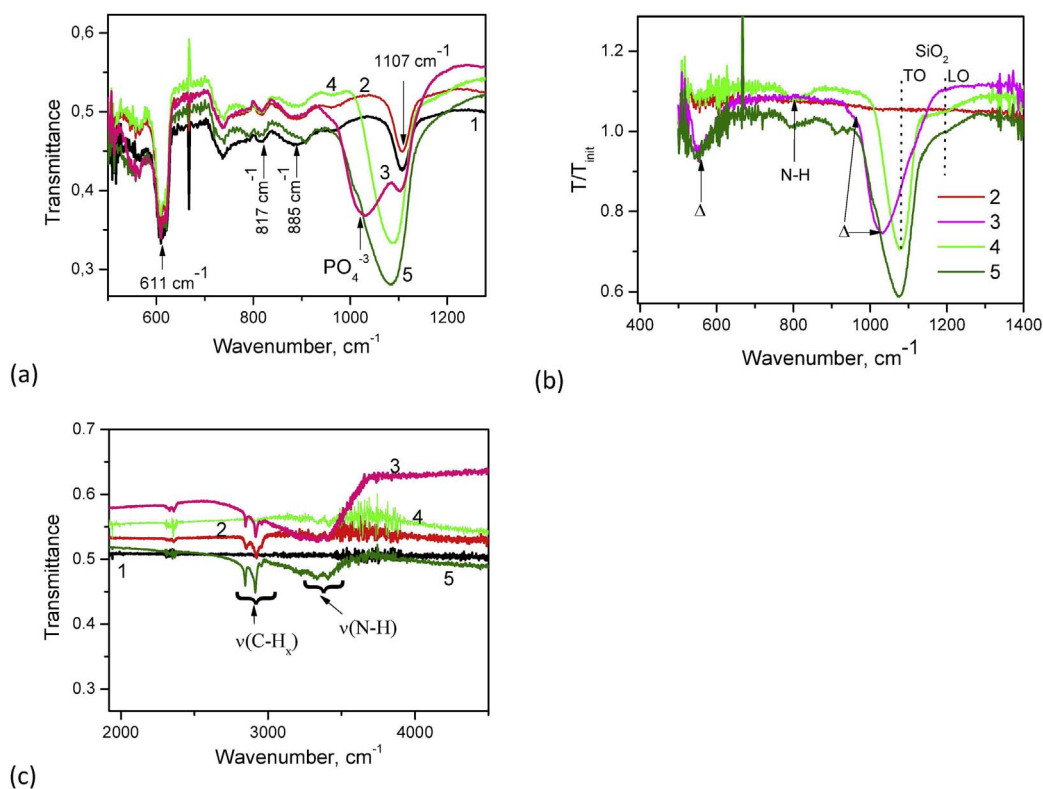
Fig. 7. Transmission IR spectra of initial and ultrasonically processed Si samples: Curve 1 (black) – initial state; Curve 2 (red) – Si1 after cavitation processing; Curve 3 (pink) - previous sample monthly stored in SBF solution; Curve 4 (green) – Si2 after cavitation processing with the following thermal annealing (at 1100 °C for 2 h); Curve 5 (olive) – previous sample monthly stored in SBF solution.

Optical bands associated with HA formation depicted as Δ in Fig.7b. (For interpretation of the references to colour in this figure legend, the reader is referred to the web version of this article.)

References

[1] H. Zimmermann, Integrated Silicon Optoelectronic, 2nd ed., Springer, Berlin, 2010.

[2] J.P. Mailoa, et al., A 2-terminal perovskite/silicon multijunction solar cell enabled by a silicon tunnel junction, Appl. Phys. Lett. 106 (2015) (121105–4).

[3] D.P. McMeekin, et al., A mixed-cation lead mixed-halide perovskite absorber for tandem solar cells, Science 351 (2016) 151–155.

[4] S. Albrecht, et al., Monolithic perovskite/silicon-heterojunction tandem solar cells processed at low temperature, Energy Environ. Sci. 9 (2016) 81–88.

[5] M. Stutzmann, et al., Direct biofunctionalization of semiconductors: a survey, Phys. Status Solidi (a) 203 (14) (2006) 3424–3437.

[6] W. Peng, et al., Silicon surface modification and characterization for emergent photovoltaic applications based on energy transfer, Chem. Rev. (2015), http://dx.doi.org/10.1021/acs.chemrev.5b00085.

[7] J. Escorihuela, H. Zuilhof, Rapid surface functionalization of hydrogen-terminated silicon by alkyl Silanols, J. Am. Chem. Soc. (2017), http://dx.doi.org/10.1021/jacs.7b01106.

[8] J.H. Bang, K. Suslick, Applications of ultrasound to the synthesis of nanostructured materials, Adv. Mater. 22 (2010) 1039–1059.

[9] R.K. Savkina, Recent progress in semiconductor properties engineering by ultrasonication, Recent Pat. Electr. Eng. 6 (2013) 157–172.

[10] R.K. Savkina, et al., Sonosynthesis of microstructures array for semiconductor photovoltaics, Mater. Sci. Semicond. Process. 37 (2015) 179–184.

[11] R.K. Savkina, et al., Silicon substrate strained and structured via cavitation effect for photovoltaic and biomedical application, Nanoscale Res. Lett. 11 (2016) 183.

[12] R.K. Savkina, A.B. Smirnov, Nitrogen incorporation into GaAs lattice as a result of the surface cavitation effect, J. Phys. D. Appl. Phys. 43 (42) (2010) 425301–425307.

[13] L.D. Rozenberg, Sources of High-Intensity Ultrasound (Ultrasonic Technology), Vol. 1 Springer Science & Business Media, 1969, pp. 223–315.

[14] R.K. Savkina, A.B. Smirnov, Structured Silicon Surface via Cavitation Processing for the Photovoltaic and Biomedical Application, Chapter 24 in Springer Proceedings in Physics, Vol. 183 (2016), pp. 291–303 (ISBN: 978-3-319-30736-7).

[15] S.B. Cho, et al., Dependence of apatite formation on silica gel on its structure: effect of heat treatment, J. Am. Ceram. Soc. 78 (1995) 1769–1774.

[16] I. Horcas, et al., WSxM: A software for scanning probe microscopy and a tool for nanotechnology, Rev. Sci. Instrum. 78 (2007) 013705–013705-8.

[17] M. Virot, et al., Crystalline silicon under acoustic cavitation: from mechanoluminescence to amorphization, J. Phys. Chem. C 116 (2012) 15493–15499.

[18] F. Oestlund, et al., Brittle-to-ductile transition in uniaxial compression of silicon pillars at room temperature, Adv. Funct. Mater. 19 (2009) 2439–2444.

[19] K.R. Weninger, C.G. Camara, S.J. Putterman, Observation of bubble dynamics

[20] within luminescent cavitation clouds: Sonoluminescence at the nano-scale, Phys. Rev. 63 (2000) (016310-1–016310-7).

[20] A.J. Kenyon, et al., The origin of photoluminescence from thin films of silicon-rich silica, J. Appl. Phys. 79 (12) (1996) 9291–9300.

[21] T. Shimizu-Iwayama, et al., Visible photoluminescence in Si⁺-implanted silica glass, J. Appl. Phys. 75 (1994) 7779–7783.

[22] D. Nesheva, et al., Raman scattering and photoluminescence from Si nanoparticles in annealed SiOx thin films, J. Appl. Phys. 92 (8) (2002) 4678–4683.

[23] M.N. Polyanskiy, Refractive index database, Available at http://refractiveindex.info.

[24] X.S. Zhao, et al., Carrier-induced strain effect in Si and GaAs nanocrystals, Appl. Phys. Lett. 65 (1994) 2033–2035.

[25] R.P. Wang, et al., Raman spectral study of silicon nanowires: high-order scattering and phonon confinement effects, Phys. Rev. B 61 (24) (2000) 16827–16832.

[26] B. Lafuente, et al., The power of databases: the RRUFF project, in: T. Armbruster, R.M. Danisi (Eds.), Highlights in Mineralogical Crystallography, Berlin, Germany, W. De Gruyter, 2015, pp. 1–30.

[27] G.C. Serghiou, W.S. Hammack, Pressure induced amorphization of wollastonite (CaSiO₃) at room temperature, J. Chem. Phys. 98 (12) (1993) 9830–9834.

[28] M. Handke, Vibrational spectra, force constants, and Si—O bond character in calcium silicate crystal structure, Appl. Spectrosc. 40 (6) (1986) 871–877.

[29] S.E. Stein "Infrared Spectra" by NIST mass spec data center, in NIST Chemistry WebBook, NIST Standard Reference Database Number 69, Eds. P.J. Linstrom and W. G. Mallard, National Institute of Standards and Technology, Gaithersburg MD, 20899, doi: http://dx.doi.org/10.18434/T4D303, (retrieved October 1, 2017).

[30] L.L. Hench, H.A. Paschall, Histochemical responses at a biomaterials interface, J. Biomed. Mater. Res. 5 (1974) 49–64.

[31] J.H. Ahire, et al., Highly luminescent and nontoxic amine-capped nanoparticles from porous silicon: synthesis and their use in biomedical imaging, ACS Appl. Mater. Interfaces 4 (2012) 3285–3292.

[32] A. Shiohara, et al., Chemical reactions on surface molecules attached to silicon quantum dots, J. Am. Chem. Soc. 132 (1) (2010) 248–253.

[33] M.K. Weldon, et al., Initial H₂O-induced oxidation of Si (100), Phys. Rev. Lett. 79 (1997) 2851–2854.

[34] Christian Rey, et al., Resolution-enhanced fourier transform infrared spectroscopy study of the environment of phosphate ions in the early deposits of a solid phase of calcium-phosphate in bone and enamel, and their evolution with age. I: investigations in the ν₄ PO₄ domain, Calcif. Tissue Int. 46 (1990) 384–394.

[35] R. Chakraborty, et al., Synthesis of calcium hydrogenphosphate and hydroxyapatite coating on SS316substratethroughpulsedelectrodeposition, Mater. Sci. Eng. C 69 (2016) 875–883.